ELSEVIER

Physics of the Earth and Planetary Interiors 107 (1998) 83–95

PHYSICS OF THE EARTH AND PLANETARY INTERIORS

Liquidus phase relations in the system MgO–$MgSiO_3$ at pressures up to 25 GPa—constraints on crystallization of a molten Hadean mantle

Dean C. Presnall *, Yi-Hua Weng, Cheney S. Milholland [1], Michael J. Walter [2]

Department of Geosciences, University of Texas at Dallas, Richardson, TX 75083-0688, USA

Received 20 October 1995; revised 20 May 1996; accepted 25 July 1996

Abstract

An understanding of the details of the crystallization history of a Hadean magma ocean requires a knowledge of liquidus phase relations of the mantle at very high pressures. The system MgO–$MgSiO_3$ is a good simplified chemical model of the mantle and provides a foundation for study of more complex systems that approximate the composition of the mantle more closely. We present a determination of the pressure–temperature univariant curve for the reaction $Mg_2SiO_4 + MgSiO_3 =$ Liquid at pressures up to 16.5 GPa, new data on the change in composition of the eutectic liquid with pressure, and a pressure–temperature projection of univariant and invariant equilibria in the system MgO–$MgSiO_3$ at pressures up to 25 GPa. With increasing pressure, the eutectic curve between Mg_2SiO_4 and $MgSiO_3$ encounters five invariant points as follows: orthoenstatite + clinoenstatite + forsterite + liquid, 11.6 GPa, 2150°C; clinoenstatite + majorite + forsterite + liquid, 16.5 GPa, 2240°C; majorite + forsterite + modified spinel + liquid, 16.6 GPa, 2245°C; majorite + perovskite + modified spinel + liquid, 22.4 GPa, 2430°C; and perovskite + modified spinel + periclase + liquid, 22.6 GPa, 2440°C (last two points from data of [Gasparik, T., 1990a. Phase relations in the transition zone. J. Geophys. Res. 95, 15751–15769]). Above 22.6 GPa, no form of Mg_2SiO_4 is stable at liquidus temperatures, and the melting reaction changes to periclase + perovskite = liquid. The composition of the eutectic liquid, in wt.%, varies with pressure in a nearly linear fashion from 21% Mg_2SiO_4, 79% $MgSiO_3$ at 2 GPa to 32% Mg_2SiO_4, 68% $MgSiO_3$ at 16.5 GPa, and reaches its maximum enrichment in Mg (45% Mg_2SiO_4, 55% $MgSiO_3$) at 22.6 GPa. These data are consistent with experimental data on natural peridotite compositions indicating that perovskite and magnesiowüstite would be the main phases to crystallize in the deeper parts of a mantle magma ocean. Published partition coefficient data show that fractional crystallization of these two phases in the lower mantle would produce an upper mantle with C1 chondrite normalized Ca/Al and Ca/Ti weight ratios of 2.0–2.3, far higher than primitive upper mantle estimates of 1.1–1.25 and 0.86–1.06, respectively. However, Ca-perovskite, which would crystallize in small amounts in the lower mantle, is such a powerful sink for Ca that Ca/Al and Ca/Ti enrichment of the

* Corresponding author.

[1] Present address: 1 Summer Haven, Madisonville, LA 70447, USA.

[2] Present address: Institute for Study of the Earth's Interior, Okayama University, Misasa, Japan.

PII S0031-9201(97)00126-X

upper mantle could be suppressed. We conclude that extensive fractional crystallization of a deep magma ocean is not at present proscribed by element partitioning arguments.

Keywords: $MgO–MgSiO_3$; Hadean mantle; Liquidus phase relations

1. Introduction

In order to understand the details of the early melting and crystallization history of the Earth (e.g., Ohtani, 1985; Agee and Walker, 1988), liquidus phase relations of the mantle at very high pressures must be known. The system $MgO–MgSiO_3$ is the most fundamental starting point for development of an understanding of these phase relations. Here we present a determination of the pressure–temperature univariant curve corresponding to the eutectic between Mg_2SiO_4 and $MgSiO_3$ at pressures up to 16.5 GPa. We also provide new data on the change in composition of this eutectic with pressure. These data are then combined with other published results for the system $Mg_2SiO_4–MgSiO_3$ to construct a pressure–temperature projection of invariant and univariant equilibria in the system $MgO–MgSiO_3$ at pressures up to 25 GPa. We then discuss how these phase relations bear on the crystallization behavior of a molten Hadean mantle. In particular, we examine element partitioning arguments that have been used to argue against extensive fractional crystallization of a deep magma ocean.

2. Previous work

Bowen and Andersen (1914) determined the incongruent melting temperature of enstatite to be 1557°C, which is 1562°C when adjusted to the 1968 International Practical Temperature Scale (IPTS-68) (Anonymous, 1969), and located the liquid composition at 60.9 wt.% SiO_2. These results were confirmed by Chen and Presnall (1975), who determined the temperature to be 1559°C (IPTS-68) and the liquid composition to be 60.6 wt.% SiO_2. The essential features of liquidus phase relations at one atmosphere appear to be very firmly established.

Chen and Presnall (1975) determined the location of the univariant curve for the equilibrium assemblage, enstatite + forsterite + liquid, up to 2.5 GPa. They did not determine the changing composition of the liquid but estimated the pressure at which enstatite first melts congruently to be approximately 0.13 GPa. Liu and Presnall (1990), on the basis of their data at 20 kbar and the earlier data of Chen and Presnall (1975), estimated the composition of the eutectic to be 19.8 wt.% Mg_2SiO_4, 80.2 wt.% $MgSiO_3$ at about 2.3 GPa. At 3, 7, 15, and 20 GPa, Kato and Kumazawa (1985, 1986, 1990) located the eutectic at 15.4, 27.1, 39.4, and 40.8 wt.% Mg_2SiO_4, respectively. Presnall and Gasparik (1990) located the forsterite–majorite eutectic at 16.5 GPa, 2240°C, and 34 wt.% Mg_2SiO_4. Gasparik (1990a) found the modified spinel–majorite–perovskite–liquid invariant point at 22.4 GPa, 2430°C, and the modified spinel–perovskite–periclase–liquid invariant point at 22.6 GPa, 2450°C. At the latter invariant point, he gave the composition of the eutectic as 40–50 wt.% Mg_2SiO_4.

These earlier studies have consistently shown that the composition of the eutectic between Mg_2SiO_4 and $MgSiO_3$ shifts toward Mg_2SiO_4 as pressure increases. The eutectic curve is intersected by the orthoenstatite–clinoenstatite, clinoenstatite–majorite, and modified spinel–forsterite transitions at high pressures (Presnall and Gasparik, 1990; Presnall and Walter, 1993), and possibly by the protoenstatite–high clinoenstatite and high clinoenstatite–orthoenstatite transitions at low pressures (Gasparik, 1990b). Because the various polymorphs of $MgSiO_3$ have different thermodynamic properties, the rate of change in the composition of the eutectic with pressure would be expected to show discontinuities at these transitions. However, existing data are too sparse to identify any discontinuities. We provide additional data on the location of the eutectic at 2 GPa and from 9.7 to 16.5 GPa that bear on this issue.

3. Experimental procedure

All multianvil experiments were done with the split-sphere apparatus (UHP-2000) at the University

of Alberta, Canada, using procedures identical to those described in Presnall and Walter (1993). Octahedrons with a 10 mm edge length and made from 95% MgO, 5% Cr_2O_3 were used with WC cubes having 5 mm truncations. The pressure cell consisted of a $LaCrO_3$ cylindrical heater, a W3Re/W25Re thermocouple positioned axially within the heater, and a Re sample capsule. Thermocouple emf was not corrected for pressure. All experimental assemblies were loaded into the apparatus immediately after being heated for 1 h at 1000°C in argon. The pressure calibration is the same as that described by Presnall and Walter (1993), and is based on the coesite–stishovite transition at 9.3 GPa, 1150°C (Yagi and Akimoto, 1976) and the clinoenstatite–majorite transition at 16.5 GPa, 2150°C (Presnall and Gasparik, 1990). These fixed points tie the reported pressures directly to the calibration used by Gasparik (1989). Sample capsules were positioned with the hot zone of the furnace slightly displaced toward the thermocouple junction, which was located directly on top of the capsule. Temperatures of phase boundaries were then determined with an estimated uncertainty of ± 30°C by using the temperature contours within the capsule given by Presnall and Gasparik (1990, figure 2). The validity of this estimated uncertainty is supported by the fact that a smooth curve in pressure–temperature space for the eutectic melting reaction, forsterite + enstatite = liquid, can be drawn through all the data (Fig. 1). For the piston-cylinder experiments, the procedures described by Presnall et al. (1978), as modified by Liu and Presnall (1990) were followed. These include the use of glass–talc pressure cell assemblies, W5Re/W26Re thermocouples, containment of samples in Pt capsules dried for 1 h at 1050°C immediately prior to the experiment, hot piston-out initial set-up procedures, and no friction correction of the pressure. Oxide mixtures for the multianvil experiments were fired for 2 h at 1650°C in a Pt crucible, quenched, crushed to a powder, and then taken through this same sequence a second time. This was followed by recrystallization at 1450°C–1500°C for 2 h. Compositions for the piston-cylinder runs were fired once at about 1630°C, quenched, crushed, and held at 1000–1050°C several times for 10–30 min each until recrystallized. Runs were examined optically in polished sections cut parallel to the axis of the cylindrical capsule. Electron microprobe analyses were done on the JEOL 8600 instrument at the University of Texas at Dallas. The distinction between orthoenstatite and clinoenstatite was not independently confirmed in this study; the identification of these polymorphs was assumed on the basis of the previously determined stability limits (Presnall and Gasparik, 1990). Fluorescence colors under the electron microprobe beam were

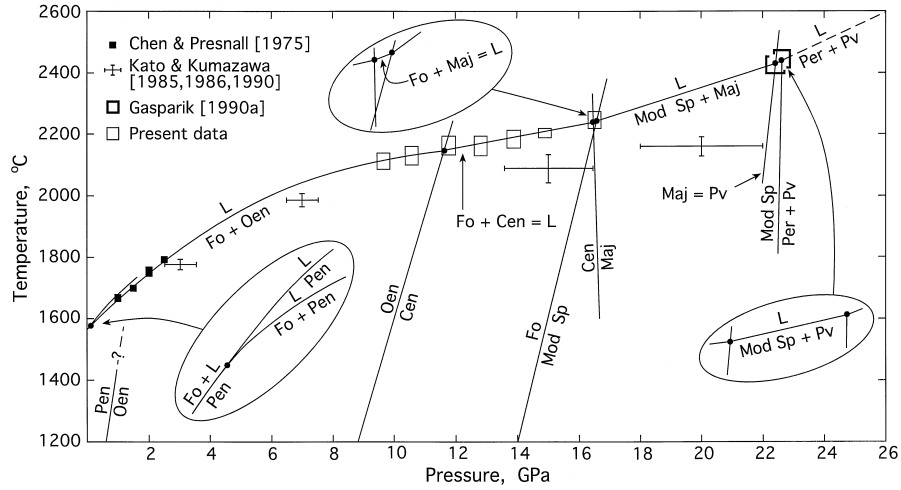

Fig. 1. Eutectic melting curve for the reaction $Mg_2SiO_4 + MgSiO_3$ = Liquid. Estimated experimental uncertainty is indicated by size of the symbols. Fo, forsterite; Mod Sp, modified spinel; Pen, protoenstatite; Oen, orthoenstatite; Cen, clinoenstatite; Maj, majorite; Pv, perovskite; L, liquid.

used to distinguish majorite (barely visible) from clinoenstatite (bright pale blue), and forsterite (dim purple) from modified spinel (bright green). Also, forsterite is slightly brighter than modified spinel in backscattered electron images. Quenched liquids always produced a fine intergrowth of quench-crystals. Compositions of these liquids were determined by averaging a large number of broad beam (5 μm) microprobe analyses.

4. Reversal experiments

Table 1 shows reversal experiments done at 2 GPa, one pair of experiments for dissolution and crystallization of forsterite and a second for dissolution and crystallization of enstatite. In each experiment, the sample was held on one side of the eutectic for 30 min. Then, without taking the sample out of the apparatus, the temperature was changed to the other side of the eutectic and held for an additional 30 min. In all cases, the expected assemblage for the final temperature was found. All the piston-cylinder experiments were held at temperature for 2 h (Table 2), much longer than required for equilibrium.

Many of the runs at higher pressures using the multianvil press were held at temperature for at least 30 min. Run times for the remainder are 15–20 min, but temperatures are 300–500°C higher (Table 3) than those of the piston-cylinder experiments. Also, the data are internally consistent even though run times vary by a factor of four. Therefore, we believe that equilibrium was also attained for all the multianvil experiments.

5. Mg_2SiO_4–$MgSiO_3$ eutectic melting curve

Fig. 1 shows the Mg_2SiO_4–$MgSiO_3$ eutectic melting curve up to the limit of its existence at 22.6 GPa. The curve is drawn through the data of Chen and Presnall (1975) and their estimate of 0.13 GPa for the position of the singular point at which the liquid composition coincides with $MgSiO_3$, our new data at 2 GPa and 9.6 to 16.5 GPa, and two points from Gasparik (1990a) at 22.4 and 22.6 GPa. Data by Kato and Kumazawa (1985, 1986, 1990) lie at systematically lower temperatures and the temperature difference increases with pressure (Fig. 1). Even without the data of Gasparik (1990a), the 20 GPa point of Kato and Kumazawa (1986, 1990) would be inconsistent with our data at lower pressures because Schreinemakers' rules force the curve, modified spinel + majorite = liquid, to have a steeper positive slope than the curve, forsterite + majorite = liquid, which in turn must have a steeper slope than the curve, forsterite + clinoenstatite = liquid. We have no explanation for these discrepancies, but in view of the good consistency between our data and those of Gasparik (1990a), we believe the temperatures of the 15 and 20 GPa points by Kato and Kumazawa (1986) are too low.

At pressures above 2 GPa, the eutectic curve in Fig. 1 encounters five invariant points. In order of increasing pressure, they are: orthoenstatite + clinoenstatite + forsterite + liquid, 11.6 GPa, 2150°C; clinoenstatite + majorite + forsterite + liquid, 16.5 GPa, 2240°C; majorite + forsterite + modified spinel + liquid, 16.6 GPa, 2245°C; majorite + perovskite + modified spinel + liquid; 22.4 GPa, 2430°C; and perovskite + modified spinel + periclase + liquid; 22.6 GPa, 2440°C. The last two

Table 1
Reversal experiments at 2.0 GPa

Mixture (wt.%)	Initial T (°C)	Final T (°C)	Phases
44MgO, 56SiO_2	1760	1710	Fo + En
	1710	1760	Fo + Liq
43MgO, 57SiO_2	1760	1710	Fo + En + Liq
	1710	1760	Liq

All runs held at initial T for 30 min and then at final T for 30 min.

Table 2
Piston-cylinder experiments at 2 GPa

Mixture (wt.%)	T (°C)	Phases[a]
45MgO, 55SiO_2	1735	Fo + En
	1740	Fo + Liq
	1745	Fo + Liq
44MgO, 56SiO_2	1740	Fo + En
	1745	Fo + En
	1750	Fo + Liq
43.5MgO, 56.5SiO_2	1730	Fo + En
	1735	En + Liq
	1745	En + Liq

All runs are 2 h in duration.
[a] Fo, forsterite; En, enstatite; Liq, liquid.

Table 3
Multianvil experiments

Run	Mixture[a]	Contact phases[b]	P (GPa)	T (°C)		Time (min)
				Nominal	Boundary[c]	
490	60En, 40Fo	Oen, Fo	9.7	2060	2120 (OenFo/L)	30
507	80En, 20Fo	Oen	9.7	2060	2110 (OenFo/L)	20
488	60En, 40Fo	Oen, Fo	10.6	2080	2130 (OenFo/L)	30
486	60En, 40Fo	Cen, Fo	11.8	2100	2165 (CenFo/L)	30
484	60En, 40Fo	Fo	12.8	2145	2165 (CenFo/L)	20
496	60En, 40Fo	Cen, Fo	13.9	2100	2185 (CenFo/L)	30
397	40En, 60Fo	Fo	14.9	2170	2190 (CenFo/L)	15
481	60En, 40Fo	Cen	14.9	2190	2190 (CenFo/L)	20
399	80En, 20Fo	Cen, Fo	14.9	2170	2230 (CenFo/L)	60
501	60En, 40Fo	Ms, Maj, Fo	16.5	2200	2260 (MsMajFo/L)	20

[a] Compositions given as wt.% $MgSiO_3$ (En) and Mg_2SiO_4 (Fo).
[b] Crystalline phases in contact with liquid. Because of a strong temperature gradient, the cooler parts of all runs also displayed the subsolidus assemblage and sometimes phases in other textural configurations (see notes). Oen, orthoenstatite; Cen, clinoenstatite; Maj, majorite; Fo, forsterite; Ms, modified spinel; L, liquid. Clinoenstatite was not distinguished from orthoenstatite in the run products, but the appropriate polymorph is listed on the basis of its known stability field.
[c] In all cases, the boundary temperature is taken as the isotherm separating the quench-crystal region (no glass was ever observed) from equilibrium crystals. Because of textural complications (see notes), one of the subsolidus phases was sometimes not observed to be in contact with the quench-crystal region.
Notes:
Run 397: quench-crystal region separated from subsolidus region by 250–500 μm thick layer of monomineralic forsterite. Temperature control ± 15°C.
Run 399: quench-crystal region separated from medium grained subsolidus region by a 25–50 μm thick layer consisting mainly of coarse clinoenstatite and minor forsterite. Temperature initially controlled at about $+20$°C (first 10 min) and thereafter at the set point. Control for last 30 min ± 5°C.
Run 481: quench-crystal region separated from medium grained subsolidus region by 80 μm thick layer of monomineralic clinoenstatite (in contact with quench-crystal region) underlain by 80 μm thick monomineralic layer of forsterite (in contact with subsolidus region). Temperature control ± 7°C.
Run 484: quench-crystal region separated from medium grained subsolidus region by 100 μm thick layer of monomineralic forsterite. Temperature control mostly ± 10°C with a few maximum excursions of ± 20°C.
Run 486: quench-crystal region separated from medium grained subsolidus region by a 200–400 μm thick layer of coarse forsterite + clinoenstatite (in contact with quench crystal region) underlain by 50–100 μm thick layer of coarse forsterite (in contact with subsolidus region). Temperature control mostly ± 10°C with two brief excursions of -25°C and one of $+13$°C.
Run 488: quench-crystal region separated from medium grained subsolidus region by 50–100 μm thick layer of forsterite + orthoenstatite. Temperature control ± 10°C except for two excursions of 13°C (one up, one down) at beginning of run.
Run 490: quench-crystal region separated from subsolidus region by 30–100 μm thick layer of coarse forsterite + orthoenstatite. Temperature control ± 10°C for first 15 min, then ± 2°C for final 15 min.
Run 496: quench-crystal region separated from medium grained subsolidus region by 25–50 μm thick layer of coarse forsterite + clinoenstatite. Temperature control mostly ± 15°C but ± 2°C for final 5 min.
Run 501: very thin (20 μm) layer of coarse forsterite + modified spinel + majorite separating quench crystal region from medium grained subsolidus region. Temperature control ± 7°C.
Run 507: quench-crystal region separated from medium grained subsolidus region by 100–200 μm thick layer of monomineralic orthoenstatite. A temperature excursion of $+15$°C occurred at 5 min and was followed by close (± 3°C) control for the final 10 min.

of these invariant points are from the data of Gasparik (1990a). He listed the temperature of the last invariant point as 2450°C, but because the last two points are very close in pressure (Fig. 1), we have made a slight downward adjustment of the temperature of the latter to 2440°C. The invariant point at 22.6 GPa marks the upper pressure limit of the eutectic curve. At higher pressures, no form of Mg_2SiO_4 is stable at liquidus temperatures, and the melting reaction changes to periclase + perovskite = liquid. The pressures of the second and third invariant points are so close (16.5 and 16.6 GPa) that the

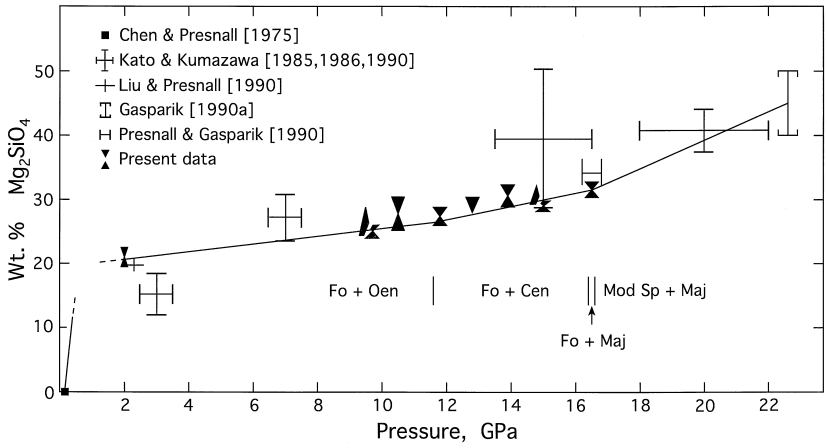

Fig. 2. Composition of liquid along the eutectic melting curve of Fig. 1. Wt.% Mg_2SiO_4 refers to the join Mg_2SiO_4–$MgSiO_3$. Size of symbols indicates estimated experimental uncertainty. For present data, hourglass symbols indicate a liquid in contact with both Mg_2SiO_4 and $MgSiO_3$, wedges pointing upward indicate a liquid in contact with $MgSiO_3$, and the wedge pointing downward indicates a liquid in contact with Mg_2SiO_4 (see Table 1). Symbols at 9.7 and 14.9 GPa are separated slightly in pressure to avoid overlapping. Vertical bars indicate transition pressures of crystalline phase assemblages at the solidus. Abbreviations as in Fig. 1.

relative order of their pressures is not resolvable experimentally.

Fig. 2 shows data from various sources on the composition of the eutectic between Mg_2SiO_4 and $MgSiO_3$ as a function of pressure. Our new data consist of one point determined with a piston-cylinder apparatus at 2.0 GPa and several points determined in the pressure range 9.6 to 16.5 GPa with a multianvil press. The point at 2.0 GPa was determined in the classical way by making starting compositions at closely spaced intervals and determining the primary phase. In this way, the eutectic is firmly bracketed at 21% Mg_2SiO_4, 79% $MgSiO_3$ between the compositions 43.5% MgO, 56.5% SiO_2 and 44% MgO, 56% SiO_2 (Table 2). Points at higher pressures using the multianvil press are based on electron microprobe analyses of liquids that quenched to fine intergrowths of quench crystals. Each composition (Table 4) is based on an average of a large number of broad-beam microprobe analyses. These analyses usually show low totals that range as low as 97%. Focused spot analyses that avoid cracks, however, show totals that cluster around 100%. Therefore, the low broad-beam totals are attributed to attenuation of the electron beam by cracks (Sweatman and Long, 1969), and the values reported in Table 4 are normalized to 100%. Elements other than Mg and Si were not found.

Starting compositions for runs 507 and 399 (Table 3) lie in the primary (liquidus) phase field of enstatite; in all other cases, the primary phase is forsterite. Note that the crystalline phase assemblage in contact with the liquid is commonly different from the primary phase. This counterintuitive result is due to saturation gradient chemical diffusion in a temperature gradient, a process explained in detail by Lesher and Walker (1988) and Presnall and Walter (1993). As pointed out by Presnall and Walter (1993), the data given in Table 3 emphasize the need to exercise

Table 4
Microprobe analyses of quench-crystal areas

Run	Spots analyzed[a]	Mg_2SiO_4[b] (wt.%)
490	15	25.0 ± 1.0
507	15	26.8 ± 2.2
488	25	27.9 ± 2.6
486	25	27.4 ± 1.5
484	27	29.3 ± 1.3
496	25	30.7 ± 1.7
481	30	30.8 ± 1.2
399	12	29.1 ± 0.9
501	20	31.6 ± 1.2

[a] Beam size for run 501 was 30 μm. Beam size for all other runs was 5 μm.
[b] Normalized to $Mg_2SiO_4 + MgSiO_3 = 100\%$. Uncertainty is standard error of the mean.

caution when interpreting melting experiments in which a strong temperature gradient exists.

Fig. 2 shows pressures at which phase changes occur along the solidus curve. At these pressures, changes in the slope of the composition vs. pressure curve would be expected, and the curve is drawn as a sequence of straight segments with slope discontinuities at these pressures. There is no thermodynamic reason requiring the segments to be straight, but the data are not sufficiently constraining to determine the existence of curved lines. The segments are not fitted mathematically but are drawn so that they lie within the estimated uncertainty bracket at each pressure. The most striking change in slope occurs near the low pressure end of the curve and is required by the single point we have determined at 2 GPa. A slope discontinuity associated with a phase change along the solidus below 2 GPa seems unavoidable in view of the high reliability of the point determined at 2 GPa and the precisely known composition of the incongruently melting liquid at 1 atm (Bowen and Andersen, 1914; Chen and Presnall, 1975). This result is consistent with the proposal of Gasparik (1990b) that high clinoenstatite intersects the solidus in this pressure range. If his proposal is correct, two discontinuities in slope would occur below 2 GPa.

Fig. 3 shows a pressure–temperature projection of invariant and univariant equilibria for the system $MgO–MgSiO_3$ at pressures up to 25 GPa. The estimated melting curve of $MgSiO_3$ perovskite on this diagram requires comment. We show this curve with the same dT/dP slope as that determined by Ito and Katsura (1992) at 21–25 GPa, but at temperatures about 120°C higher. The explanation for this modification is as follows. Fig. 3 shows that in every case where data exist at pressures > 10 GPa, the curvature of univariant lines that involve a liquid phase is so small that the curves are linear within experimental error. Furthermore, linear representations of these determined curves are always consistent with the requirements of Schreinemakers' rules for the relative slopes of univariant lines at invariant points. No data exist for the curve, majorite = liquid, which would connect the clinoenstatite = liquid curve determined by Presnall and Gasparik (1990) at lower pressures with the perovskite = liquid curve deter-

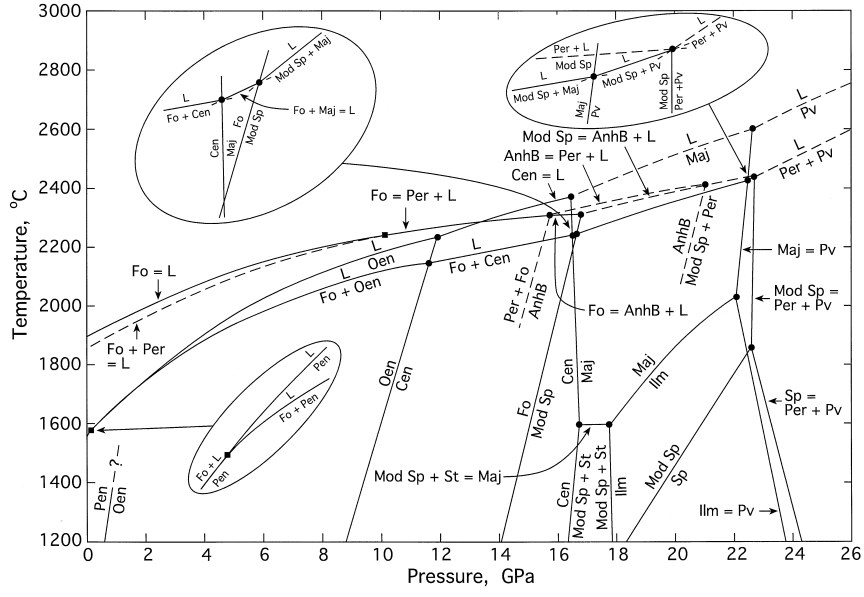

Fig. 3. Pressure–temperature projection for the system $MgO–MgSiO_3$ showing all univariant curves and invariant points except the melting curve of periclase. Filled circles are invariant points. Filled squares are singular points. St, stishovite; Ilm, ilmenite; Sp, spinel; AnhB, anhydrous B; other abbreviations as in Fig. 1. The diagram is compiled from Presnall (1995) (figures 8 and 14) and references therein, and Fig. 1. The diagram is drawn in an internally consistent way given best estimates of the positions of univariant lines; but in several places, the details of the topology depend on precise locations of curves that are not experimentally resolvable at present.

mined by Ito and Katsura (1992) at higher pressures. If the majorite = liquid curve follows the pattern of all the other curves in being nearly linear, its dT/dP slope at the clinoenstatite–majorite–liquid invariant point would be less than that of the orthoenstatite = liquid curve and would therefore violate Schreinemakers' rules. The data of Presnall and Gasparik (1990) and Ito and Katsura (1992) are both internally consistent; but in order to join the two data sets so that Schreinemakers' rules are not violated, the temperatures of Presnall and Gasparik must be lowered or those of Ito and Katsura must be raised. We prefer to raise the temperatures of Ito and Katsura because lowering the temperatures of Presnall and Gasparik would also require lowering the temperatures of Gasparik (1990a) and Presnall and Walter (1993), on which other melting curves in Fig. 3 are based. For present purposes, the choice is unimportant, but we make this adjustment to produce a topologically correct phase diagram.

6. Crystallization of a deep magma ocean

Recent models for the Hadean history of the Earth usually invoke collision of the proto-Earth with a planetesimal about one to three times the mass of Mars. Such a collision is thought to have formed the Moon and would result in significant or complete melting of the Earth (e.g., Hartman and Davis, 1975; Wetherill, 1985, 1990; Melosh, 1990). After separation of the metallic core, perhaps by gravitational segregation of immiscible iron and silicate liquids (Sasaki and Nakazawa, 1986; Stevenson, 1990), the resulting silicate magma ocean would crystallize from the core–mantle boundary upward to form the mantle. A variety of models based on an assumption of fractional crystallization have been proposed (e.g., Ohtani, 1985; Agee and Walker, 1988; Agee, 1990, 1993; Herzberg and Gasparik, 1991). However, Tonks and Melosh (1990) and Solomatov and Stevenson (1993) have argued, on fluid dynamic grounds, that fractional crystallization would not occur except possibly during the final stage of the cooling history at depths < 300 km. Also, on the basis of element partitioning data at high pressures, it has been argued either that a deep magma ocean involving most of the Earth's mantle never existed (Kato et al., 1988a,b) or that such an ocean existed but did not experience significant fractional crystallization (McFarlane and Drake, 1990; Drake et al., 1993; McFarlane et al., 1994).

In order to address the issue of whether or not fractional crystallization occurred, we focus on Ca, Ti, and Al. Because these are refractory lithophile elements, they would resist volatilization during major melting events such as that caused by a giant impact (Ringwood, 1979). Therefore, condensed solar materials affected only by melting and volatilization processes would be expected to show relatively constant ratios of these elements. However, if melting events were followed by fractional crystallization, these ratios may show significant variation. Given that (1) the Earth accreted from materials with chondritic refractory element abundance ratios, as is generally assumed, and (2) Ca, Ti, and Al are excluded from the core because of their lithophile character, then ratios of these elements for an initially liquid mantle would be chondritic. In the absence of fractional crystallization, these ratios for the uppermost mantle would remain chondritic upon cooling and solidification. However, if fractional crystallization occurred, deviations from the chondritic ratio could occur, depending on the relevant crystal/liquid partition coefficients. Other refractory lithophile elements (Sc, rare earth elements) are also potentially interesting as indicators of fractional crystallization, but we focus on Ca, Al, and Ti because of the availability of crystal/liquid partitioning data for these elements. Two other relatively refractory lithophile elements, Si and Mg, are less useful because they are slightly volatile, with Si being the more volatile of the two. Thus, the higher Mg/Si ratio of these elements in the upper mantle relative to chondrites could be caused by one or more prior volatilization events (Hart and Zindler, 1986), rather than by crystal/liquid fractionation of the magma ocean. For this reason, we exclude Mg and Si from the present discussion.

Phase relations for the system $MgO–MgSiO_3$ provide a preliminary basis for discussing the crystallization of a deep magma ocean. Fig. 3, in conjunction with Fig. 2, can be used to construct the essential features of any desired temperature-composition or pressure-composition phase diagram for the system $MgO–MgSiO_3$. When phase relations as

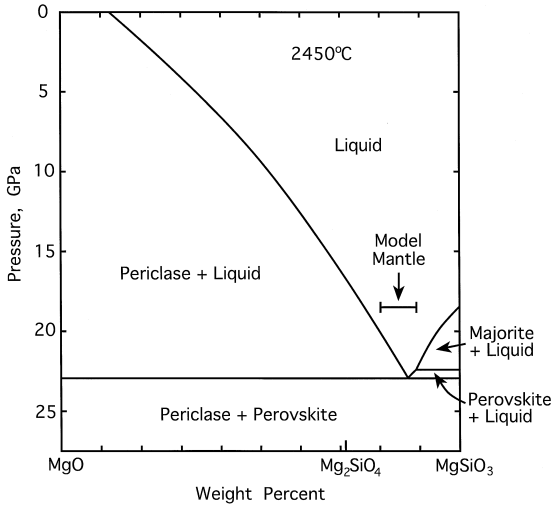

Fig. 4. Pressure-composition section for the system $MgO–MgSiO_3$ at 2450°C, as derived from Fig. 3.

a function of depth in the mantle are desired, a pressure-composition section is more useful than the classical temperature-composition section. Fig. 4 shows a pressure-composition section at 2450°C. It approximates, with sufficient accuracy for present purposes, phase relations with increasing depth for a magma ocean with an adiabatic temperature gradient that has cooled to 2450°C at the crystallizing base of the ocean. For the model mantle composition shown, the diagram indicates that perovskite and periclase (magnesiowüstite in the real ocean) would be the dominant crystallizing phases in the lower mantle at about 23 GPa. At higher temperatures, Figs. 3 and 4 show that the floor of the magma ocean would lie at greater pressures, and the field of majorite + liquid would shrink and then disappear completely at about 2600°C. This would leave only perovskite and periclase as crystallizing phases in the deep mantle.

When it is considered that Fig. 3 shows phase relations for only a binary system, these results are remarkably consistent with experimental data on natural peridotites, which show that perovskite and magnesiowüstite would crystallize at or near the liquidus from peridotite magma at pressures greater than about 22 GPa (Ohtani et al., 1986; Ohtani and Sawamoto, 1987; Ito and Takahashi, 1987; Agee, 1990; Zhang and Herzberg, 1994). Of the three major components, FeO, CaO, and Al_2O_3, that are missing, CaO is perhaps the most important because Ca-perovskite has been found to crystallize from peridotite at 22.5 to 25 GPa (Ito and Takahashi, 1987; Zhang and Herzberg, 1994) and from model peridotite in the system $CaO–MgO–SiO_2$ at 18.2 and 18.8 GPa (Gasparik, 1990a). This phase would not occur in the binary system but must occur in the lower mantle because it is the only phase that would contain Ca in the amounts required to make up the presumed peridotitic bulk composition. In the pressure range from about 15 to 22 GPa, phase relations are complex and poorly understood, but appear to involve the crystallization of Ca-perovskite in the upper part of this range (Zhang and Herzberg, 1994) and possibly a phase having the composition of diopside and called CM by Gasparik (1990a) in the lower part of this range. However, phase CM has not been reported in experiments on natural peridotites. Then, at pressures below about 15 GPa, diopside becomes stable (Zhang and Herzberg, 1994). Thus, for the entire pressure range of the mantle except possibly for the poorly understood 15–18 GPa range, a Ca-rich phase would crystallize.

The amounts of Ca-rich phases crystallized would change as a function of pressure and extent of fractionation of the magma ocean, and these amounts cannot be accurately determined at present because the controlling liquidus phase relations are poorly known for much of the upper mantle and almost completely unknown through most of the lower mantle. However, the amounts would be small simply because the amount of Ca in the bulk mantle is small. Also, existing data (Zhang and Herzberg, 1994) indicate that both diopside at lower pressures and Ca-perovskite at high pressures are late-crystallizing phases that appear roughly 100°C below the liquidus. On the assumption of equilibrium crystallization of a fertile mantle composition without fractionation, mass balance requires the amount of Ca-perovskite in the upper part of the lower mantle to be roughly 5%.

Fig. 4 shows that the crystallizing phase proportions of Mg-perovskite and periclase in a deep magma ocean, at least in the upper part of the lower mantle, would be roughly 85% Mg-perovskite, 15% periclase by weight. Also, Ito and Katsura (1992) have shown that addition of FeO to this system at 24 GPa changes the crystallizing proportions of Mg-per-

ovskite (Mg# = 0.96) and magnesiowüstite (Mg# = 0.93) only slightly toward a higher Mg-perovskite proportion. These data generally support the use by McFarlane et al. (1994) of the proportions, 80% Mg-perovskite, 20% magnesiowüstite in their calculations. However, no information is available for the position of the eutectic at higher pressures.

We initially consider the consequences of crystallizing Mg-perovskite and magnesiowüstite alone in the lower mantle without Ca-perovskite, as done in previous discussions. Then, we examine the consequences of including Ca-perovskite. For Mg-perovskite/liquid and magnesiowüstite/liquid partition coefficients for Ca, Ti and Al, we use the recent values of McFarlane et al. (1994) at 24.5 GPa, 2650°C because these data are from relatively long runs of 5–13 min and are the most likely to represent equilibrium values (but see Walker and Agee (1989) for a discussion of potential problems). Use of the McFarlane et al. (1994) data indicates that crystallization of the lower mantle (depths > 660 km) as a mixture of 85% perovskite, 15% magnesiowüstite would yield an upper mantle residual liquid (roughly one third the volume of the total mantle) with both a Ca/Al and Ca/Ti ratio of 2.1, when normalized to C1 chondrites. Fig. 5 shows that this value is far higher than the range of Ca/Al ratios for primitive upper mantle lherzolite, a result essentially the same as that calculated by McFarlane et al. (1994), except for the slightly different proportions of crystallizing phases and the larger percentage of crystallization. A similar relationship holds for the Ca/Ti ratio, although primitive upper mantle values for the Ca/Ti ratio are slightly lower at 0.86–1.06.

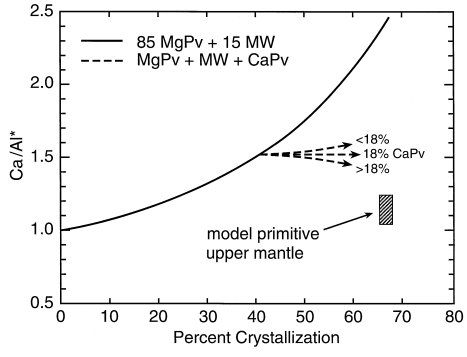

Fig. 5. Ca/Al (weight ratio, C1 chondrite normalization indicated by asterisk) of residual liquids produced by fractional crystallization of 85% Mg-perovskite, 15% magnesiowüstite. After 40% crystallization, the dashed lines show the effects of adding different percentages of Ca-perovskite crystallization with proportionate reduction in the amounts of Mg-perovskite and magnesiowüstite. Box for model primitive upper mantle compositions includes estimates by Maaløe and Aoki (1977), Ringwood (1979), Jagoutz et al. (1979), Wänke (1981), Palme and Nickel (1985), and Presnall, in press.

In deeper parts of the magma ocean closer to the core–mantle boundary, both the proportions of crystallizing phases and the partition coefficients are not known; but if the McFarlane et al. (1994) partition coefficients are assumed to hold, then extreme limits for the Ca/Al ratio of the upper mantle would vary only between 2.1 (100% Mg-perovskite crystallization) and 2.0 (70% Mg-perovskite, 30% magnesiowüstite crystallization). Corresponding extreme limits for the Ca/Ti ratio would be 2.3–2.0. Thus, the Ca/Al and Ca/Ti ratios in the residual magma forming the upper mantle are not sensitive to the proportions of Mg-perovskite and magnesiowüstite crystallizing in the lower mantle.

If Mg-perovskite melts incongruently at higher pressures, as suggested by Ito and Katsura (1992), fractional crystallization would produce initial crystallization of magnesiowüstite followed by Mg-perovskite. This would produce a layer of magnesiowüstite at the base of the mantle and a much thicker layer of Mg-perovskite above it (see also Agee, 1990). The upper mantle would still be the product of crystallization of some high ratio of Mg-perovskite to magnesiowüstite, and the Ca/Al and Ca/Ti ratios calculated above would apply. The partition coefficient data of Ohtani et al. (1989) and Drake et al. (1993) indicate that crystallization of majorite in the lower part of the upper mantle would increase the Ca/Al ratio of the remaining melt even further.

Evaluation of the effects of Ca-perovskite crystallization is difficult. We are aware of three studies in which compositions of coexisting Ca-perovskite and liquid have been determined (Table 5). In one case (Ito and Takahashi, 1987), the Ca-perovskite contains 8.5% La_2O_3, which Ito and Takahashi attribute to contamination from the furnace. In another (Kato et al., 1988a), the Ca-perovskite analysis shows an oxide sum of only 90% and the Ca-perovskite coexists with a basaltic liquid, not an ultramafic liquid. In

Table 5
Ca-perovskite/liquid partition coefficients

Ca	Al	Ti	Reference
4.7	1.0	0.8	Ito and Takahashi (1987)
2.4	0.6	2.7	Kato et al. (1988a)
3.7	3.0	5.1	Gasparik and Drake (1995)
4.0	9.7	26.2	Gasparik and Drake (1995)

the third case, the Ca-perovskite contains 8.5% Sm and coexists with strongly hydrous liquids containing $< 24\%$ SiO_2 and 13–29% F (Gasparik and Drake, 1995, table 1, liquids L2 and L3). Table 5 shows fairly good consistency for the Ca partition coefficient determined in these studies, but the data for Al and Ti are strongly divergent. Acknowledging these problems, we use the data of Ito and Takahashi (1987) at 25 GPa and about 2500°C as the best available data for Ca-perovskite in equilibrium with an ultramafic melt. These data support the inference from stoichiometry that Ca-perovskite must be a powerful sink for Ca.

Detailed quantitative modeling is precluded by a lack of data, not only on the partition coefficients as a function of pressure and temperature, but also on the proportion of Ca-perovskite that would crystallize and the point at which it would appear in the crystallization sequence. However, the magnitude of the possible effect on the Ca/Al ratio of an upper mantle residual liquid can be understood by assuming that Ca-perovskite appears after 40% crystallization of the mantle. If the 85:15 proportions of Mg-perovskite and magnesiowüstite are reduced proportionately to allow for the crystallization of 18% Ca-perovskite, the strong enrichment trend of Ca/Al would be completely arrested (Fig. 5). For a smaller proportion of Ca-perovskite, the Ca/Al ratio would continue upward but at a lower rate. For a larger proportion, the Ca/Al ratio would curve back down toward the chondritic ratio. Essentially the same trends would occur for the Ca/Ti ratio.

If fractional crystallization started in the lower mantle and proceeded to the point of initial crystallization of Ca-perovskite, prior crystallization of Mg-perovskite and magnesiowüstite would have altered the remaining magma to a more Ca-rich composition. Therefore, it would be reasonable to expect crystallization of a Ca-rich phase through most or all of the remaining crystallization history. These phases would be diopside at low pressures and possibly the CM phase of Gasparik (1990a) at intermediate pressures. Such crystallization has the potential to suppress the Ca/Al and Ca/Ti ratios in the uppermost mantle. Therefore, we conclude that proscription of a large amount of fractional crystallization on the basis of these element ratios is premature.

Figure 8 of McFarlane et al. (1994) indicates that fractional crystallization of Mg-perovskite and magnesiowüstite produces an Al/Ti ratio for the upper mantle about 15% greater than primitive upper mantle compositions. If the partition coefficients of Ito and Takahashi (1987) are roughly correct, crystallization of Ca-perovskite would not strongly affect the Al/Ti ratio. This suggests that McFarlane et al. (1994) may be correct that the 15% difference is significant and that extensive fractional crystallization was suppressed. However, because of large uncertainties in partition coefficients for Ca-perovskite (Table 5), poorly understood proportions of phases crystallized, and unknown effects caused by crystallization of other phases at shallower depths in the mantle, we believe that this difference is insufficient for a robust conclusion.

We find that none of the three potentially definitive ratios, Ca/Al, Ca/Ti, or Al/Ti, can be used, in the present state of knowledge, to convincingly deny large amounts of fractional crystallization of a molten mantle. This conclusion contains no implication of support for extensive fractional crystallization; we merely consider the situation at present to be poorly constrained by element partitioning data.

Acknowledgements

We thank T. Gasparik for providing some of the ceramic parts used in the pressure cell assemblies. The multianvil experiments were done at the University of Alberta, Canada, supported by NSERC Infrastructure grant CII0006947. Also, Presnall thanks the geology faculty at the University of Alberta for additional financial support and Professor Ikuo Kushiro for financial support at the Institute for Study of the Earth's Interior, Okayama University, Misasa, Japan, where final manuscript revisions were

completed. We thank J. A. Dalton, D. Walker, and L. Yale for thoughtful reviews of the manuscript. This research was supported by Texas Advanced Research Program grants 3927, 009741-007, 00741-066, and 009741-044, and National Science Foundation grants EAR-8418685, EAR-8816044, and EAR-9219159.

References

Agee, C.B., 1990. A new look at differentiation of the Earth from melting experiments on the Allende meteorite. Nature 346, 834–837.

Agee, C.B., 1993. High-pressure melting of carbonaceous chondrite. J. Geophys. Res. 98, 5419–5426.

Agee, C.B., Walker, D., 1988. Mass balance and phase density constraints on early differentiation of chondritic mantle. Earth Planet. Sci. Lett. 90, 144–156.

Anonymous, 1969. The international practical temperature scale of 1968. Metrologia 5, 35–44.

Bowen, N.L., Andersen, O., 1914. The binary system $MgO–SiO_2$. Am. J. Sci. 37, 487–500.

Chen, C.H., Presnall, D.C., 1975. The system $Mg_2SiO_4–SiO_2$ at pressures up to 25 kilobars. Am. Mineral. 60, 398–406.

Drake, M.J., McFarlane, E.A., Gasparik, T., Rubie, D.C., 1993. Mg-perovskite/silicate melt and majorite garnet/silicate melt partition coefficients in the system $CaO–MgO–SiO_2$ at high temperatures and pressures. J. Geophys. Res. 98, 5427–5431.

Gasparik, T., 1989. Transformation of enstatite–diopside–jadeite pyroxenes to garnet. Contrib. Mineral. Petrol. 102, 389–405.

Gasparik, T., 1990a. Phase relations in the transition zone. J. Geophys. Res. 95, 15751–15769.

Gasparik, T., 1990b. A thermodynamic model for the enstatite–diopside join. Am. Mineral. 75, 1080–1091.

Gasparik, T., Drake, M.J., 1995. Partitioning of elements among two silicate perovskites, superphase B, and volatile-bearing melt at 23 GPa and 1500–1600°C. Earth Planet. Sci. Lett. 134, 307–318.

Hart, S.R., Zindler, A., 1986. In search of a bulk-Earth composition. Chem. Geol. 57, 247–267.

Hartman, W.K., Davis, D.R., 1975. Satellite-sized planetesimals and lunar origin. Icarus 24, 504–515.

Herzberg, C.T., Gasparik, T., 1991. Garnet and pyroxenes in the mantle: a test of the majorite fractionation hypothesis. J. Geophys. Res. 96, 16263–16274.

Ito, E., Katsura, T., 1992. Melting of ferromagnesian silicates under the lower mantle conditions. In: Syono, Y., Manghnani, M.H. (Eds.), High-Pressure Research: Applications to Earth and Planetary Sciences. Terrapub., Tokyo/American Geophysical Union, Washington, DC, pp. 315–322.

Ito, E., Takahashi, E., 1987. Melting of peridotite at uppermost lower-mantle conditions. Nature 328, 514–517.

Jagoutz, E., Palme, H., Baddenhausen, H., Blum, K., Cendales, M., Dreibus, G., Spettel, B., Lorenz, V., Wänke, H., 1979. The abundances of major, minor and trace elements in the earth's mantle as derived from primitive ultramafic nodules. In: Proc. Tenth Lunar Planet. Sci. Conf. Pergamon, New York, pp. 2031–2050.

Kato, T., Kumazawa, M., 1985. Effect of high pressure on the melting relation in the system $Mg_2SiO_4–MgSiO_3$: Part I. Eutectic relation up to 7 GPa. J. Phys. Earth 33, 513–524.

Kato, T., Kumazawa, M., 1986. Melting and phase relations in the system $Mg_2SiO_4–MgSiO_3$ at 20 GPa under hydrous conditions. J. Geophys. Res. 91, 9351–9355.

Kato, T., Kumazawa, M., 1990. High pressure effect on the melting relation in the system $Mg_2SiO_4–MgSiO_3$: Phase transitions in the constituent phases and differentiation by melting in the Earth's mantle. In: Marumo, F. (Ed.), Dynamic Processes of Material Transport and Transformation in the Earth's Interior. Terrapub., Tokyo, pp. 277–308.

Kato, T., Ringwood, A.E., Irifune, T., 1988a. Experimental determination of element partitioning between silicate perovskites, garnets and liquids: constraints on early differentiation of the mantle. Earth Planet. Sci. Lett. 89, 123–145.

Kato, T., Ringwood, A.E., Irifune, T., 1988b. Constraints on element partition coefficients between $MgSiO_3$ perovskite and liquid determined by direct measurements. Earth Planet. Sci. Lett. 90, 65–68.

Lesher, C.E., Walker, D., 1988. Cumulate maturation and melt migration in a temperature gradient. J. Geophys. Res. 93, 10295–10311.

Liu, T.-C., Presnall, D.C., 1990. Liquidus phase relationships on the join anorthite-forsterite–quartz at 20 kbar with applications to basalt petrogenesis and igneous sapphirine. Contrib. Mineral. Petrol. 104, 735–742.

Maaløe, S., Aoki, K., 1977. The major element composition of the upper mantle estimated from the composition of lherzolites. Contrib. Mineral. Petrol. 63, 161–173.

McFarlane, E.A., Drake, M.J., 1990. Element partitioning and the early thermal history of the Earth. In: Newsom, H.E., Jones, J.H. (Eds.), Origin of the Earth. Springer, New York, pp. 135–150.

McFarlane, E.A., Drake, M.J., Rubie, D.C., 1994. Element partitioning between Mg-perovskite, magnesiowüstite, and silicate melt at conditions of the Earth's mantle. Geochim. Cosmochim. Acta 58, 5161–5172.

Melosh, H.J., 1990. Giant impacts and the thermal state of the early Earth. In: Newsom, H.E., Jones, J.H. (Eds.), Origin of the Earth. Oxford Univ. Press, New York, pp. 69–83.

Ohtani, E., 1985. The primordial terrestrial magma ocean and its implication for stratification of the mantle. Phys. Earth. Planet. Int. 38, 70–80.

Ohtani, E., Sawamoto, H., 1987. Melting experiment on a model chondritic mantle composition at 25 GPa. Geophys. Res. Lett. 14, 733–736.

Ohtani, E., Kato, T., Sawamoto, H., 1986. Melting of a model chondritic mantle to 20 GPa. Nature 322, 352–353.

Ohtani, E., Kawabe, I., Moriyama, J., Nagata, U., 1989. Partitioning of elements between majorite garnet and melt and implications for petrogenesis of komatiite. Contrib. Mineral. Petrol. 103, 263–269.

Palme, H., Nickel, K.G., 1985. Ca/Al ratio and composition of the Earth's upper mantle. Geochim. Cosmochim. Acta 49, 2123–2132.

Presnall, D.C., 1995. Phase diagrams of Earth-forming minerals. In: Ahrens, T.J. (Ed.), Mineral Physics and Crystallography, A Handbook of Physical Constants. Am. Geophys. Union, Washington, DC, pp. 248–268.

Presnall, D.C., Gasparik, T., 1990. Melting of enstatite ($MgSiO_3$) from 10 to 16.5 GPa and the forsterite (Mg_2SiO_4)–majorite ($MgSiO_3$) eutectic at 16.5 GPa: implications for the origin of the mantle. J. Geophys. Res. 95, 15771–15777.

Presnall, D.C., Walter, M.J., 1993. Melting of forsterite, Mg_2SiO_4, from 9.7 to 16.5 GPa. J. Geophys. Res. 98, 19777–19783.

Presnall, D.C., Dixon, S.A., Dixon, J.R., O'Donnell, T.H., Brenner, N.L., Schrock, R.L., Dycus, D.W., 1978. Liquidus phase relations on the join diopside–forsterite–anorthite from 1 atm to 20 kbar: their bearing on the generation and crystallization of basaltic magma. Contrib. Mineral. Petrol. 66, 203–220.

Presnall, D.C., in press. Crystallization of a Hadean terrestrial magma ocean. In: Gupta, A.K. (Ed.), Mantle Dynamics and its Relations to Earthquake and Volcanism. Nat. Acad. Sci. India.

Ringwood, A.E., 1979. Origin of the Earth and Moon. Springer-Verlag, New York, 295 pp.

Sasaki, S., Nakazawa, K., 1986. Metal-silicate fractionation in the growing Earth: energy source of the terrestrial magma ocean. J. Geophys. Res. 91, 9231–9238.

Solomatov, V.S., Stevenson, D.J., 1993. Nonfractional crystallization of a terrestrial magma ocean. J. Geophys. Res. 98, 5391–5406.

Stevenson, D.J., 1990. Fluid dynamics of core formation. In: Newsom, H.E., Jones, J.H. (Eds.), Origin of the Earth. Oxford Univ. Press, New York, pp. 231–249.

Sweatman, T.R., Long, J.V.P., 1969. Quantitative electron-probe microanalysis of rock-forming minerals. J. Petrol. 10, 332–379.

Tonks, W.B., Melosh, J., 1990. The physics of crystal settling and suspension in a turbulent magma ocean. In: Newsom, H.E., Jones, J.H. (Eds.), Origin of the Earth. Oxford Univ. Press, New York, pp. 151–174.

Walker, D., Agee, C., 1989. Partitioning 'equilibrium', temperature gradients and constraints on Earth differentiation. Earth Planet. Sci. Lett. 96, 49–60.

Wänke, H., 1981. Constitution of terrestrial planets. Phil. Trans. R. Soc. London, Ser. A 303, 287–302.

Wetherill, G.W., 1985. Giant impacts during the growth of the terrestrial planets. Science 228, 877–879.

Wetherill, G.W., 1990. Formation of the Earth. Annu. Rev. Earth Planet. Sci. 18, 205–256.

Yagi, T., Akimoto, S., 1976. Direct determination of coesite–stishovite transition by in situ X-ray measurements. Tectonophysics 35, 259–270.

Zhang, J., Herzberg, C., 1994. Melting experiments on anhydrous peridotite KLB-1 from 5.0 to 22.5 GPa. J. Geophys. Res. 99, 17729–17742.